Efficient Power Transfers in Piezoelectric Energy-Harvesting Switched-Inductor Chargers

Siyu Yang, *Graduate Student Member, IEEE*, and Gabriel A. Rincón-Mora, *Fellow, IEEE*

***Abstract*—Piezoelectric energy-harvesting transducers can draw power from motion that can be used to energize a host of wireless microsystems that sense, process, and share vital information across a network. Since these tiny devices draw little power, maximizing the power they transfer is critical. Synchronized-discharge circuits are popular in this space because they can collect all the charge from the transducer and increase drawn power. Pre-charging the transducer can draw even more power, but only as much as voltage-breakdown limits allow. This paper examines how synchronous discharge circuits can output the most power possible from tiny difficult-to-overdamp piezoelectric transducers. Measurements will show how pre-charge symmetry and energy-transfer schemes alter the power drawn from the transducer and the power lost in the system. The charges are tested with a 10 × 50 × 1-mm³ 15-nF transducer generates up to 10 µA at 100 Hz and the breakdown voltage of the harvester circuit is 3 V. Indirect and direct transfers with symmetric pre-charges output 21% and 43% more power with the same inductor than the 4.2 µW that indirect transfers without pre-charge can generate. Generating the highest power possible is important because, with more power, tiny piezoelectric transducers can power wireless microsensors with greater functionality and longer lifetime.**

Keywords— Energy harvesting, piezoelectric, synchronous discharge, switched inductor, output power, charger, maximum power point, ohmic loss.

I. Piezoelectric Energy-Harvesting Chargers

Wireless microsensors embedded in homes, bridges, vehicles, and human beings can sense, process, and share information across a network to save energy, money, and lives [1]–[2]. Since their small footprint cannot carry a large battery to sustain all the functionality or a long lifetime, they often draw energy from their ambient [3]. Piezoelectric transducers [4]–[5] have enjoyed some success in powering the microsensors due to the omnipresence of the vibration, their moderate to high power density, and the ease of integration. The charger, as shown in Fig. 1, rectifies, transfers, and feeds piezoelectric power directly into the battery [6]. The voltage regulator then supplies the electronic loads of the system.

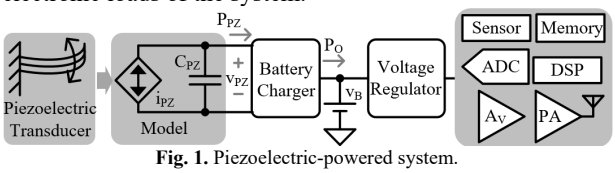

Fig. 1. Piezoelectric-powered system.

Tiny piezoelectric transducers can only convert a small portion of the vibration energy into electrical domain. Therefore, managing the voltage across the transducer v_{PZ} to draw as much power as possible is critical in a piezoelectric charger. Synchronous discharges using switched-inductor [7]–[12] can collect all the charge generated by the transducer to increase drawn power compared with full bridge [13] or half bridge, and drawn power can be further increased by pre-charging [10]. However, a portion of the drawn power is lost on the charger, and it also sets some limits on the operation. This paper compares the drawn power, loss, limits, and most importantly output power using different ways to pre-charge and to transfer the power for the optimum power stage of the charger. Section II compares symmetrical pre-charge and asymmetrical pre-charge, and Section III compares direct and indirect inductor energy transfers. Section IV compares the schemes experimentally, and Section V draws conclusions.

II. Pre-Charge Symmetry

When the piezoelectric transducer vibrates, charge is created and alternates on its two plates [4]. A full bridge rectifier can steer the charge to the rectifying capacitor asynchronously, when the voltage across the transducer $|v_{PZ}|$ surpasses the rectified voltage. Similarly, a half bridge can steer charge to the rectifying capacitor, when v_{PZ} is higher than the rectified voltage. Studies have shown that both the full bridge and half bridge can ideally produce the same power [7]–[8]. However, both schemes only collect a small portion of the generated charge, and the drawn power is low.

A. Synchronous Discharges

Synchronous discharge lets the transducer charge the capacitor by the open circuit voltage $\Delta v_{PZ(OC)}$ across a half cycle (0–5 ms or a positive half cycle, and 5–10 ms for a negative half cycle, etc. in Fig. 2), and collects the charge at the end of the half cycle (at 5 ms, 10 ms, etc), as the solid gray trace shows in Fig. 2. Note that the vibration cycle is much longer than the time it takes to charge the battery, so it appears instantaneous. The drawn power is

$$P_{PZ(NPC)} = 0.5 C_{PZ} \Delta v_{PZ(OC)}^{\ 2} \left(2 f_{VIB}\right), \tag{1}$$

where f_{VIB} is the vibration frequency.

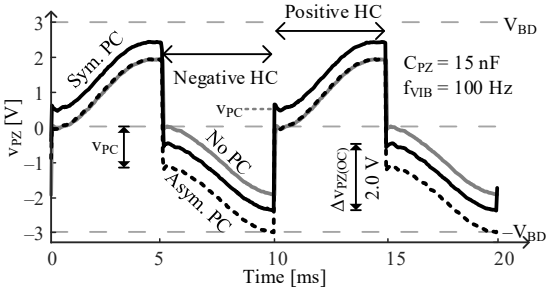

Fig. 2. Piezoelectric voltage for no pre-charging, and symmetric and asymmetric pre-charging.

B. Symmetrical Pre-Charges

Drawn power can be further increased by pre-charging (PC) the capacitor before a half cycle starts. As the black trace

shows in Fig. 2 [10], the capacitor voltage v_{PZ} is at the pre-charging voltage v_{PC} before each half cycle. At the end of the half cycle when v_{PZ} peaks, some of the charge on the capacitor is recycled to the other direction of the capacitor, and the rest is used to charge the battery. The net energy into the battery in each half cycle is the energy at the end of the half cycle minus the energy at the start of the half cycle. Therefore, the power is

$$P_{PZ(SPC)} = 0.5C_{PZ}\left[\left(\Delta v_{PZ(OC)} + v_{PC}\right)^2 - v_{PC}^{\ 2}\right]\left(2f_{VIB}\right). \quad (2)$$

Energy can transfer between C_{PZ} and L_X, and between the inductor and the battery, using equivalent circuits in Fig. 3. The inductor voltage v_L is the capcitor's voltage vC in Fig. 3(a), and is battery voltage v_B in Fig. 3(b). Energy transfer completely between C_{PZ} and L_X cross a quarter of the LC oscillation cycle using circuit in Fig. 3(a), and v_B can either energize or drain L_X linearly using the circuit shown in Fig. 3(b).

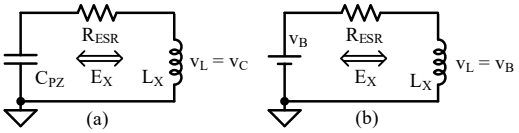

Fig. 3. Equivalent circuit for indirect transfers (a) between capacitor and inductor and (b) between battery and inductor.

The solid black trace in Fig. 4 shows the inductor current i_L for the symmetrical pre-charges. The capacitor C_{PZ} first energizes the inductor until the inductor reaches its peak $i_{L(SPK)}$ (5.000 ms to 5.002 ms). The inductor then put some of the energy back into the capacitor in the opposite direction (5.0019 ms to 5.0032 ms), and the rest of the current in the inductor charges the battery (5.0032 ms to 5.0045 ms). The pattern repeats after the negative half cycle (at 10 ms in Figs. 2 and 3), only in the negative direction.

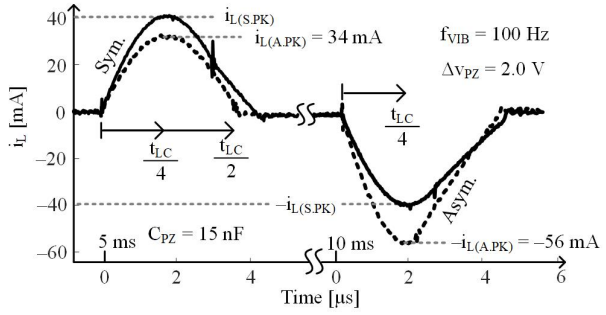

Fig. 4. Inductor current for symmetric and asymmetric transfers.

MOSFET switches are used to energize and drain the inductor to reduce footprint and losses. However, they also impose breakdown limits to the system. Therefore, the absolute value of v_{PZ}, which is $\Delta v_{PZ(OC)} + v_{PC}$, must be at or below the breakdown voltage V_{BD}. As a result, the charger can tolerate $\Delta v_{PZ(OC)}$ up to V_{BD}.

C. Asymmetrical Pre-Charges

Another way to accomplish PC is asymmetric PC introduced in [11]. Before the positive half cycle, the C_{PZ} is drained, and is charged to $\Delta v_{PZ(OC)}$ across the positive half cycle, as shown by the dotted black trace in Fig. 2. At the end of the half cycle (at 5 ms in Figs. 2 and 3), as shown in the dotted black trace in Fig. 3, the inductor energizes across a quarter LC cycle, and drains back into C_{PZ} across another quarter LC cycle (0 to 3.8 µs after 5 ms). During this time, v_{PZ} drops from $\Delta v_{PZ(OC)}$ to 0, then to $-v_{PC}$, which in this case is $-\Delta v_{PZ(OC)}$, as shown at 5 ms in Fig. 2. Across the negative half cycle, vibration again charges C_{PZ} by $\Delta v_{PZ(OC)}$ to $-(v_{PC} + \Delta v_{PZ(OC)})$. At the end of the negative half cycle, C_{PZ} energizes L_X across a quarter cycle (0.2 to 2.1 µs after 10 ms in Fig. 3), then L_X charges v_B (2.1 to 4.2 µs after 10 ms). Therefore, an asymmetrical pre-charging charger can draw

$$P_{PZ(APC)} = 0.5C_{PZ}\left(2\Delta v_{PZ(OC)}\right)^2\left(2f_{VIB}\right) = 4C_{PZ}\Delta v_{PZ(OC)}^{\ 2} f_{VIB}. \quad (3)$$

References [11] and [14] reach the same conclusion when not drawing assistance from the battery, as is the case here.

Again, the charger is subjected to breakdown limits, and the peak voltage in the negative half cycle $2\Delta v_{PZ(OC)}$ has to be below V_{BD}. If the vibration produces a $\Delta v_{PZ(OC)}$ stronger than $0.5V_{BD}$, the charger in [11] cannot accommodate it. However, a reconfiguration of the switching sequence can keep the power stage from breaking down by putting some of the energy harvested in the positive half cycle to the battery, so that the pre-charging voltage is $V_{BD} - \Delta v_{PZ(OC)}$. The operation is the same as the symmetrical pre-charge. This way, namely partial asymmetrical pre-charging, the charger can tolerate $\Delta v_{PZ(OC)}$ up to V_{BD}.

III. Energy Transfers

The previous section discusses how increasing pre-charge voltage to the extent of breakdown limit can increase drawn power. However, due to losses, not all drawn power can reach the battery. The energy transfers incur ohmic loss on the equivalent series resistance (ESR). How the energy is delivered from the capacitor C_{PZ} to the battery v_B can affect the ohmic loss. This section therefore examines the different ways an inductor can transfer energy from C_{PZ} to v_B and compares the losses.

A. Indirect

The most intuitive way to transfer energy from C_{PZ} to v_B is the indirect transfer, where the inductor L_X receives all the energy from C_{PZ}, and then transfers all the energy into v_B. The equivalent circuits shown in Fig. 3 can accomplish this. Fig. 5 shows the inductor current in an indirect transfer with the solid gray trace. C_{PZ} is connected to L_X across 0.2 µs to 2.0 µs to transfer all its energy to L_X. L_X then is connected to v_B from 2.0 µs to 3.1µs to charge v_B. A more detailed analysis of the transfer and ohmic loss can be found in [15]. It's called indirect because the C_{PZ} cannot directly transfer its energy to v_B.

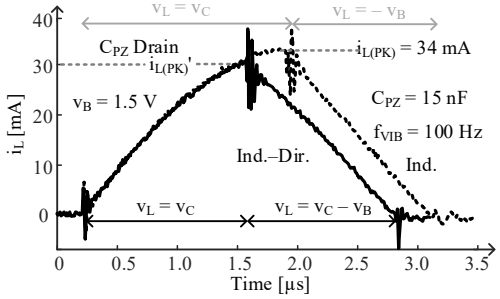

Fig. 5. Inductor current waveform for indirect, and indirect–direct transfers.

To pre-charge using an indirect transfer, there are two approaches. One is to draw assist from the battery, by using Fig. 3(b) to energize the inductor, then using Fig. 3(a) to charge C_{PZ}. The other approach is to reuse some energy in the inductor before charging the battery. This way, Fig. 3(a)

is used for more than a quarter cycle until voltage on C_{PZ} flips and reaches the pre-charge target v_{PC}, and then use Fig. 3(b) to charge the battery with the energy on L_X. The latter approach saves a transfer, therefore would have lower ohmic loss than the former.

B. Indirect–Direct

Another approach to transfer energy from C_{PZ} to v_B is to transfer a part of the energy directly to v_B. This way, the inductor L_X does not receive all the energy from C_{PZ}, and therefore has lower inductor current. This can be achieved by utilizing the circuit shown in Fig. 6 for a portion of the transfer, where the inductor voltage v_L is v_C - v_B.

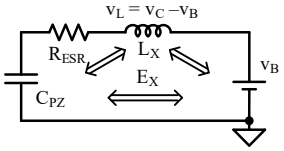

Fig. 6. Equivalent circuit for direct transfers for C_{PZ}, L_X, and v_B.

The first example we examine here is the indirect–direct transfer. The first part of the transfer uses circuit from Fig. 3(a), and the inductor current i_L rises sinusoidally, as shown by the solid black trace in Fig. 5. What's different from the indirect transfers is that the LC portion lasts shorter than a quarter LC cycle (0.2 µs to 1.6 µs in Fig. 5), and both C_{PZ} and L_X have some energy after that. Then we utilize the circuit in Fig. 6. The current flows from C_{PZ} through L_X to v_B, so v_{PZ} continues to drop. As v_{PZ} is lower than v_B, inductor current drops as well, and both inductor and capacitor drain into v_B (1.6 µs to 2.8 µs in Fig. 5).

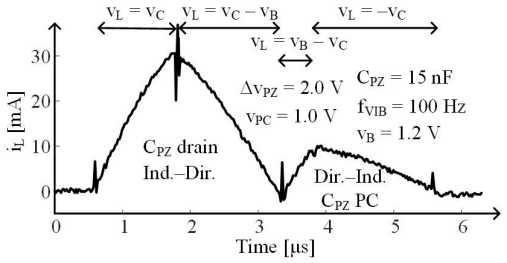

Fig. 7. i_L for indirect–direct transfers with direct–indirect pre-charging.

Because the indirect portion is less than a quarter LC cycle, the inductor does not receive all the energy from C_{PZ}. Therefore, the peak inductor current in indirect–direct transfer $i_{L(PK)}$' is lower than the indirect transfer. The total transfer time is also lower, resulting in lower ohmic loss than an indirect-only transfer. Because the ohmic loss is

$$P_R = I_{RMS}^2 R_{ESR} \left(\frac{t_X}{t_{VIB}}\right), \quad (4)$$

the total ohmic loss is lower.

To pre-charge, we need draw assist from the battery. This can be done by directly energizing both L_X and C_{PZ} with the circuit in Fig. 6 first, and then use the circuit in Fig. 3(a) to drain L_X into C_{PZ}. The inductor current waveform is shown in Fig. 7, where from 0.6 µs to 3.2 µs it depicts the indirect–direct transfer to drain C_{PZ}, and from 3.2 µs to 5.8 µs the figure shows the direct–indirect pre-charge.

C. Direct–Indirect

An alternate way to transfer part of the energy directly to v_B is the direct–indirect transfer. As the name suggests, the transfer start with a direct transfer, where C_{PZ} energizes L_X and charges v_B using the circuit in Fig. 6. The same connection is maintained until C_{PZ} is completely drained. v_B therefore must be less than half of the voltage initially on C_{PZ} to ensure C_{PZ} can be completely drained. After that, circuit in Fig. 3(b) is used to drain the energy on L_X into v_B.

The inductor current waveform for direct–indirect transfer is shown by the black trace in Fig. 8, where the direct portion is from 1.2 µs to 4.0 µs, and the indirect drain is from 4.0 µs to 5.2 µs. The indirect transfer under the same condition is also shown by the gray trace for comparison. Because the energizing voltage is $v_{PZ} - v_B$ for direct, inductor current for direct is lower than the indirect counterpart, resulting in lower ohmic loss.

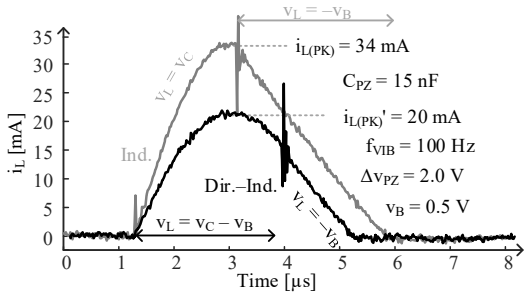

Fig. 8. Inductor current waveform for direct–indirect and indirect transfers.

In an ideal transfer, v_B must be less than half of the voltage on C_{PZ} to be able to completely drain C_{PZ} using the direct configuration. That's because v_{PZ} falls sinusoidally centered around v_B, and it can only reach 0 when $v_{PZ(PK)}$ is at least twice v_B. When $v_{PZ(PK)}$ is exactly $2v_B$, the entire transfer can be direct [11]. We denote this case v_B' and $v_{PZ(PK)}$', and call it direct only, or direct–direct. For a given $v_{PZ(PK)}$, when v_B is less than v_B', direct–indirect can be used; however, when v_B is higher than v_B', indirect–direct must be used to completely drain C_{PZ}. In other words, v_B' and $v_{PZ(PK)}$' is where direct–indirect transition to indirect–direct.

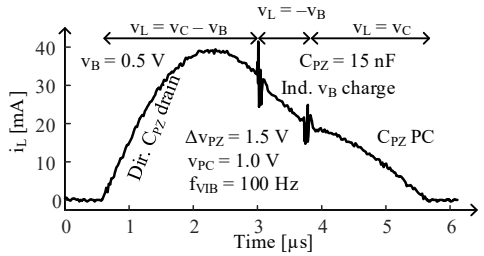

Fig. 9. Inductor current for direct–indirect transfers with pre-charging.

Pre-charges using direct–indirect transfer can be done using the same direct–indirect pre-charge after charging v_B, shown in Fig. 7. However, there is a more efficient way by not completely draining the inductor when it charges the battery. Instead, some energy is preserved to charge C_{PZ} in the opposite direction using indirect circuit in Fig. 3(a). The inductor current is shown in Fig. 9, where from 0.6 µs to 3.0 µs C_{PZ} directly charge battery and energize L_X, from 3.0 µs to 3.8 µs L_X charges v_B using Fig. 4(b), and from 3.8 µs to 5.8 µs L_X charges C_{PZ} in the negative direction.

IV. Highest Output Power

A. Prototype

The synchronous discharge without pre-charge, with symmetrical pre-charge, and with asymmetrical pre-charge

using indirect and 2 types of direct transfers are all implemented and measured using the circuit in Fig. 10. All the switches and drivers are on a 0.18-µm CMOS IC with breakdown voltage of 3.3 V. Mide V22b is the piezoelectric transducer with a size of 10 × 50 × 1 mm^3. A shaker from Bruel and Kjaer vibrates the transducer so it generates 0–3 V of open circuit peak to peak voltage $\Delta v_{PZ(OC)}$. A field programmable gate array module senses the half cycles and generates the gate signals to complete the transfers. The die and testing PCB are shown in Fig. 11, while the type and size of the switches are listed in Table I.

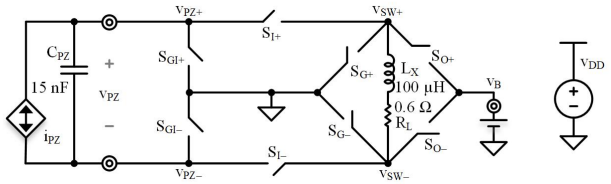

Fig. 10. Circuit for testing.

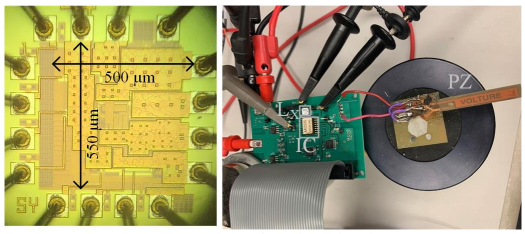

Fig. 11. Die and testing circuits.

TABLE I
MOSFET TYPE AND SIZE OF THE SWITCHES

Switch	Type	L [nm]	W [mm]	R_{MIN} [Ω]
$S_{GI+/-}$	N	350	3.8	1.2
$S_{I+/-}$	N	350	3.2	1.1
	P	300	7.2	0.93
$S_{G+/-}$	N	350	2.2	0.82
$S_{O+/-}$	P	300	4.3	1.5

Table II lists the switch configuration for all the transfers. For each mode, across the positive half cycle, S_{GPN} is closed so that the bottom plate of C_{PZ} is ground, and all other switches open so that i_{PZ} can charge C_{PZ} by $\Delta v_{PZ(OC)}$. Similarly, across the negative half cycle, S_{GPP} is closed so that the top plate of C_{PZ} is ground, and all other switches open so that i_{PZ} can charge C_{PZ} by $\Delta v_{PZ(OC)}$. The PC under the Transfer column denotes pre-charging. I's only used in the pre-charge cases and ignored in the no pre-charge ones.

B. Output Power

The power that the charger supplies v_B using no pre-charging, symmetric pre-charging indirect, asymmetric pre-charging direct, and symmetric pre-charging indirect are shown in Fig. 12 with vibration frequency of 100 Hz, open circuit voltage $\Delta v_{PZ(OC)}$ at 1.5 V, and battery voltage v_B ranging from 0.1 V to 3.0 V. All the data points are collected at its maximum power point (MPP), and the pre-charging voltage varies for each data point. The data points to the left of v_B' uses direct–indirect, and to the right of v_B' uses indirect–direct.

The figure shows that pre-charging can output more power than no pre-charging. It also shows that for symmetrical pre-charging, using direct can output almost 50% more power because of the lower ohmic losses. The reduced loss in the transfer can also allow the symmetrical pre-charging direct to have higher pre-charging voltage, resulting in additional drawn power. The figure also shows

TABLE II
SWITCHING CONFIGURATIONS FOR EACH TRANSFER MODE

Transfer Mode		Half Cycle	Transfer From		Transfer To	Switches Engaged
Indirect		+ to –		C_{PZ}	L_X	S_{GI-}, S_{I+}, S_{I-}
			PC	L_X	C_{PZ}	S_{GI+}, S_{I+}, S_{I-}
				L_X	v_B	S_{G+}, S_{O-}
		– to +		C_{PZ}	L_X	S_{GI+}, S_{I+}, S_{I-}
			PC	L_X	C_{PZ}	S_{GP-}, S_{I+}, S_{I-}
				L_X	v_B	S_{G-}, S_{B+}
Dir.	Ind. to Dir.	+ to –		C_{PZ}	L_X	S_{GI-}, S_{I+}, S_{I-}
				C_{PZ}	$L_X + v_B$	S_{GI-}, S_{I+}, S_{O-}
			PC	v_B	$L_X + C_{PZ}$	S_{GI+}, S_{P-}, S_{B+}
			PC	L_X	C_{PZ}	S_{GI+}, S_{I-}, S_{I+}
		– to +		C_{PZ}	L_X	S_{GI+}, S_{I+}, S_{I-}
				C_{PZ}	$L_X + v_B$	S_{GI-}, S_{I+}, S_{O+}
			PC	v_B	$L_X + C_{PZ}$	S_{GI-}, S_{I+}, S_{B+}
			PC	L_X	C_{PZ}	S_{GI-}, S_{I+}, S_{I-}
	Dir. to Ind.	+ to –		C_{PZ}	$L_X + v_B$	S_{GI-}, S_{I+}, S_{O-}
				$C_{PZ} + L_X$	v_B	
				L_X	v_B	S_{G+}, S_{O-}
			PC	L_X	C_{PZ}	S_{GI+}, S_{I+}, S_{I-}
		– to +		C_{PZ}	$L_X + v_B$	S_{GI-}, S_{I-}, S_{O+}
				$C_{PZ} + L_X$	v_B	
				L_X	v_B	S_{G-}, S_{O+}
			PC	L_X	C_{PZ}	S_{GI+}, S_{I+}, S_{I-}

that the symmetrical pre-charging direct has higher output power than asymmetrical pre-charging direct, because the symmetrical case charges the battery using 2 smaller energy packet each cycle, resulting in lower ohmic loss.

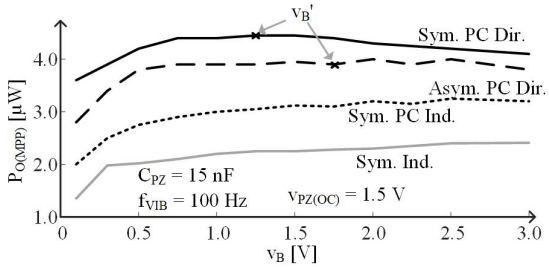

Fig. 12. Output power for symmetry and direct vs indirect across v_B.

The chargers also consumes charge loss, quiescent loss, and leakage loss. Because the inductor has to be small, and because the vibration frequency is low, ohmic loss on the inductor is the dominant loss. Fig. 12 also shows that the output power is not very sensitive to battery voltage, meaning the charger can output close to the same power regardless of the condition of the battery. That's because the peak inductor current in each transfer using synchronous discharge is not affected by v_B. It also shows that for the symmetrical pre-charging direct case, the highest output power, another way of saying lowest ohmic loss, is at the v_B', where the entire transfer is direct, confirming the theory proposed in [15].

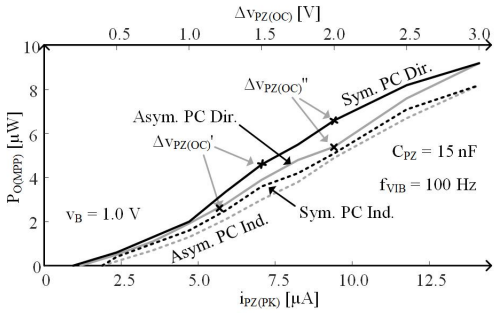

Fig. 13. Output power for symmetry and direct vs indirect.

TABLE III
RELATIVE PERFORMANCES

	JSSC [11]	TPE [12]	JSSC [13]	This Work			
Mode	Asym. PC Ind.	Sym. PC Dir.	Sym. PC Ind.	Asym. PC Ind.	Sym. PC Ind.	Asym PC Dir.	Sym. PC Dir.
C_{PZ}	15 nF	17 nF	20 nF	15 nF	15 nF	15 nF	15 nF
f_{VIB}	143 Hz	120 Hz	140 Hz	100 Hz	100 Hz	100 Hz	100 Hz
$i_{PZ(PK)}$	8.2–36 µA	3.0–33 µA	11 µA	2.3 – 14 µA	1.8 – 14 µA	1.4 – 14 µA	0.9 – 14 µA
$\Delta v_{PZ(OC)}$	1.2–5.2 V	0.5–5.5 V	1.2	0.5–3.0 V	0.4–3.0 V	0.3–3.0 V	0.2–3.0 V
V_{BD}	15 V	5.5 V	> 7.0 V	3.0 V	3.0 V	3.0 V	3.0 V
L_X	330 µH	330 µH	340 µH	100 µH	100 µH	100 µH	100 µH
P_O	2.1–53 µW	0.7–49 µW	15 µW	0 – 7.9 µW	0 – 7.9 µW	0 – 9.1 µW	0 – 9.1 µW
η_O	2.6×–3.5×	3.2×–6.8×	14×	2.8×–6.6×	2.8×–7.2×	3.3×–10.5×	3.3×–15.5×

Fig. 13 shows the maximum output power across the vibration range. The symmetrical/asymmetrical PC with direct/indirect transfers are plotted, and each data point is at its MPP. For the direct cases, $v_{PZ(OC)}$' are marked as the point where the entire transfer is direct, and the data points to the left are indirect–direct, and to the right vice versa. The figure confirm that symmetrical pre-charge with direct is the best across all the operating conditions.

C. Range

Fig. 13 also shows the operating range for the chargers. From the lower side, symmetrical PC direct, thanks to its lower ohmic loss, can start output net power with 0.2 V of $\Delta v_{PZ(OC)}$, which is the lowest among all the reported works [7]–[13]. This is significant because although vibrations are omnipresent, they are intermittent, and can be low amplitude across a long time. Therefore, outputting power from as low a vibration as possible is important to prolonging life and expanding functionality for wireless microsensors.

On the other end, because of the breakdown limit, the systems transitions from loss limited region into breakdown limited region at the $\Delta v_{PZ(OC)}$" marks on Fig. 12. For symmetrical PC, we need to lower pre-charge voltage, thereby sacrificing output power, to keep the system under safe conditions. For the asymmetrical case, $\Delta v_{PZ(OC)}$" is the highest open circuit voltage it can handle, unless the system can enter partial asymmetrical operation, and the trace to the right of $v_{PZ(OC)}$" shows the maximum output power.

Overall the charger characteristics and performance are summarized in Table III. The last row indicates the output power gain over what an ideal bridge can output, which is $0.25\Delta v_{PZ(OC)}{}^2 C_{PZ} f_{VIB}$ [7]. Even though the system is not optimized for any mode of operation, the symmetrical pre-charging direct is the best. Although other factors may impact the power garin (quality of design, different transducer, limits, etc), the theories presented in [14] – [15], and the validations here prove that symmetrical pre-charge with direct can draw the highest power with lowest losses.

V. CONCLUSITONS

Symmetrical pre-charge direct charger can output the most power to the battery and can start outputting net power from the lowest vibration. That's because directly transferring energy from the input capacitor to the battery allows the inductor to transfer more energy than it carries, reducing ohmic loss. Both the transfer time and inductor current are lower compared with indirect transfers. With lower ohmic loss, symmetrical pre-charge can operate at maximum power point at a higher pre-charge voltage, further increasing drawn power. Symmetrical pre-charge performs better than asymmetrical pre-charge because charging the battery with smaller energy packets saves ohmic loss. Therefore, a symmetrical pre-charge with direct charger could maximize the lifetime and functionality for wireless microsensors.

ACKNOWLEDGMENT

The authors would like to thank Dr. Orlando Lazaro, Dr. Andres Blanco, Dr. Jeff Moroni, and Texas Instruments for their support and sponsorship.

REFERENCES

[1] D. Puccinelli and M. Haenggi, "Wireless sensor networks: applications and challenges of ubiquitous sensing," *IEEE Circuits and Syst. Mag.*, vol. 3, no. 3, pp. 19–29, 2005.

[2] S. Roundy, P.K. Wright, and J. Rabaey, "A study of low level vibrations as a power source for wireless sensor nodes," *Comput. Commun.*, vol. 26, no. 11, pp. 1131–1144, Jul. 2003.

[3] S. Suduvalayam and P. Kulkarni, "Energy harvesting sensor nodes: Survey and implications," *IEEE Commun. Surveys Tut.*, vol. 13, no. 3, pp. 443–543 461, Jul.–Sep. 2011.

[4] A. B. A. Dow, A. Bittner, U. Schmid, and N.P. Kherani, "Design, fabrication and testing of a piezoelectric energy microgenerator," *Microsyst. Tech.*, vol. 20, no. 4–5, pp. 1035–1040, Apr. 2014.

[5] A. Hajati and S.G. Kim, "Ultra-wide bandwidth piezoelectric energy harvesting," *Applied Phys. Letters*, vol. 99, no. 8, Aug. 2011.

[6] J. Liu, H. Fang, Z. Xu, X. Mao, X. Shen, D. Chen, H. Liao, and B. Cai, "A MEMS-based piezoelectric power generator array for vibration energy harvesting," *Microelectronics J.*, vol. 39, no. 5, pp. 802–806, May 2008.

[7] G.A. Rincón-Mora and S. Yang, "Tiny piezoelectric harvesters: Principles, constraints, and power conversion," *IEEE Trans. on Circuits Syst. I*, vol. 63, no. 5, pp. 639–649, May 2016.

[8] Y.K. Ramadass and A.P. Chandrakasan, "An efficient piezoelectric energy harvesting interface circuit using a bias-flip rectifier and shared inductor," *IEEE J. of Solid-State Circuits*, vol. 45, no. 1, pp. 189–204, Jan. 2010.

[9] Y.C. Chu, I. C. Lien, and W.J. Wu, "An improved analysis of the SSHI interface in piezoelectric energy harvesting," *Smart Mater. Struct*., vol. 16, no. 6, pp. 2253–2264, Oct. 2007.

[10] S. Yang and G.A. Rincón-Mora, "Energy-harvesting piezoelectric-powered CMOS series switched-inductor bridge," *IEEE Trans. on Power Electronics*, vol. 34, no. 7, pp. 6489–6497, July 2019.

[11] D. Kwon and G.A. Rincón-Mora, "A single-inductor 0.35-µm CMOS energy-investing piezoelectric harvester," *IEEE J. of Solid-State Circuits*, vol. 49, no. 10. pp. 2277–2291, Oct. 2014.

[12] K.S. Yoon, S.W. Hong, and G.H. Cho, "Double pile-up resonance energy harvesting circuit for piezoelectric and thermoelectric materials," *IEEE J. of Solid-State Circuits*, vol. 53, no. 4, pp. 1049–1060, Apr. 2018.

[13] G. K. Ottman, H. F. Hofmann, A. C. Bhatt, and G. A. Lesieutre, "Adaptive piezoelectric energy harvesting circuit for wireless remotepower supply," *IEEE Trans. Power Electron*., vol. 17, no. 5,pp. 669–676, Sep. 2002.

[14] S. Yang and G.A. Rincón-Mora, "Optimally pre-damped switched-inductor piezoelectric energy-harvesting charger," *in Proc. IEEE Inter. New Circuits and Systems Conf.*, Vancouver, BC, 2016, pp. 1-4.

[15] S. Yang and G.A. Rincón-Mora, "Least lossy piezoelectric energy-harvesting charger", *in proc. IEEE International Midwest Cir. Syst.*, Dallas, TX, Aug. 2019.